## TOWARD UNDERSTANDING THE BOUNDARY PROPAGATION SPEEDS IN TUMOR GROWTH MODELS\*

JIAN-GUO LIU<sup>†</sup>, MIN TANG<sup>‡</sup>, LI WANG<sup>§</sup>, AND ZHENNAN ZHOU<sup>¶</sup>

Abstract. At the continuous level, we consider two types of tumor growth models: the cell density model, based on the fluid mechanical construction, is more favorable for scientific interpretation and numerical simulations, and the free boundary model, as the incompressible limit of the former, is more tractable when investigating the boundary propagation. In this work, we aim to investigate the boundary propagation speeds in those models based on asymptotic analysis of the free boundary model and efficient numerical simulations of the cell density model. We derive, for the first time, some analytical solutions for the free boundary model with pressure jumps across the tumor boundary in multidimensions with finite tumor sizes. We further show that in the large radius limit, the analytical solutions to the free boundary model in one and multiple spatial dimensions converge to traveling wave solutions. The convergence rate in the propagation speeds are algebraic in multidimensions as opposed to the exponential convergence in one dimension. We also propose an accurate front capturing numerical scheme for the cell density model, and extensive numerical tests are provided to illustrate the analytical findings.

**Key words.** tumor growth models, Brinkman model, free boundary model, front capturing scheme

AMS subject classifications. 35K55, 35B25, 76D27, 76M20, 92C50

**DOI.** 10.1137/19M1296665

1. Introduction. The invasion of solid tumors into a host tissue has been one of the most active areas for mathematical modeling. The tumor density can be influenced by concentration of nutrients, cell division, the extracellular matrix, as well as other environmental factors. There are numerous models, including individual-based models, fluid mechanical models, and free boundary models, for tumors in different scenarios [4, 6, 9, 12, 13, 20, 26]. The individual-based model is more accurate for small-scale problems while the latter two types of models are built from continuum mechanics [9, 12]. One common question is to understand the propagation speed of tumor boundaries [10, 14, 13], and it is also one of the most popular research topics for reaction diffusion equations in general [5].

Tumor expansion with a constant speed has been observed and studied in previous literature [10, 24]; however, such a phenomenon could only be observed for large-scale tumors, which leaves a natural open question: when the tumor size is not large enough,

<sup>\*</sup>Received by the editors October 30, 2019; accepted for publication (in revised form) March 2, 2021; published electronically June 1, 2021.

 $<sup>\</sup>rm https://doi.org/10.1137/19M1296665$ 

Funding: The work of the first author was partially supported by KI-Net NSF RNMS grant 11-07444 and NSF grant DMS 1812573. The work of the second author was supported by Science Challenge Project TZZT2017-A3-HT003-F and NSFC 11871340. The work of the third author was partially supported by NSF grant DMS-1903420 and NSF CAREER grant DMS-1846854. The work of the fourth author was supported by NSFC grant 11801016.

<sup>&</sup>lt;sup>†</sup>Department of Mathematics and Department of Physics, Duke University, Durham, NC 27708 USA (iliu@phy.duke.edu).

<sup>&</sup>lt;sup>‡</sup>School of Mathematics, Institute of Natural Sciences and MOE-LSC, Shanghai Jiao Tong University, Shanghai 200240, China (tangmin@sjtu.edu.cn).

 $<sup>\</sup>S$  School of Mathematics, University of Minnesota, Minneapolis, MN 55455 USA (wang8818@umn.edu).

<sup>¶</sup>Beijing International Center for Mathematical Research, Peking University, Beijing 100871, China (zhennan@bicmr.pku.edu.cn).

how does the tumor boundary propagate with time? More specifically, this consists of two levels of investigation. One is to figure out the dependence of the limiting constant speed on the model parameters, and the other one is to explore the convergence rate of the propagation speed toward the limit. In particular, it involves a subtler question, whether or not the convergence rate depends on the dimension, as is pointed out in [25].

In this paper, we investigate two types of continuous models: the cell density model, which is based on a fluid mechanical construction (see, e.g., [20, 21, 23]), and the free boundary model, which describes the geometric motion of solid tumor borders (see [13] and references therein). The cell density models carry the biggest capacity for scientific interpretations. However, due to the nonlinearity and the lack of analytical solutions, it seems impossible to find the analytical formula of the associated boundary propagation speed. Previously, the convergence of the cell density model to its incompressible limit, which is the free boundary model, has been rigorously justified [21, 23], but despite the vast interest from both the mathematics and the science community, analyzing the consistency of the propagation speeds from these models remains at the intuitive level. In this work, we aim to investigate the connections of the propagation speeds, based on numerical implementations of the cell density model, and asymptotic analysis of the free boundary model.

We specify the cell density model in the following, which is derived mainly from the assumptions that the expansion of tumor cells is driven by the cell division and the mechanical pressure [20, 25]. More precisely, we consider the following advectionreaction model as in [21, 23, 24]:

(1.1) 
$$\frac{\partial}{\partial t}\rho - C_S \nabla \cdot (\rho \nabla W) = \Phi(\Sigma, \rho), \quad \boldsymbol{x} \in \mathbb{R}^n, \quad t \in \mathbb{R}^+,$$

where  $\rho(\boldsymbol{x},t)$  is the density function of tumor cells,  $\Sigma(\rho)$  is the elastic pressure, and  $\Phi$  is the growth function. The potential W is related to the pressure  $\Sigma$  via the Brinkman model

(1.2) 
$$-C_z \Delta W + W = \Sigma, \quad \nabla W(x, t) \to \mathbf{0} \quad (|x| \to +\infty).$$

Here,  $C_S$  and  $C_z$  are parameters, relating respectively to the elasticity of cells and the bulk viscosity that models the friction between cells [24]. One can write (1.1) into the following equation:

$$\frac{\partial}{\partial t} \rho + \nabla \cdot (\rho \boldsymbol{v}) = \Phi(\Sigma, \rho) \,,$$

where  $\mathbf{v} = -C_S \nabla W$  is the velocity field field. The velocity field is curl free and the Brinkman model (1.2) is rewritten  $-C_z \Delta \mathbf{v} + \mathbf{v} = -C_S \nabla \Sigma$ . When  $C_z = 0$ , the Brinkman model recovers the Darcy's law, which says cells move in the direction of the negative pressure gradient. A lot of works have been dedicated to the case of Darcy's law; see [2, 21, 28] and the references therein. When  $C_z \neq 0$ , the dissipation in velocity due to the internal cell friction is analyzed in [23], and the authors have pointed out the theory of mixtures which allows for a general formalism combining both the Darcy's law and the Brinkman's law. Similar systems with nonlocal cell interactions and cell growth can be found in [1, 11].

To complete the cell density model, one has to specify the state equation  $\Sigma(\rho)$  and the growth function  $\Phi(\Sigma, \rho)$ . We assume that the tumor cells are modeled as viscoelastic balls and the elastic pressure is an increasing function of the population density. After neglecting cell adhesion and assuming that  $\Sigma(\rho) = 0$  when cells are not in contact, one possible choice of the state equation reads

(1.3) 
$$\Sigma = \begin{cases} 0, & \rho \le 1, \\ C_{\nu} \ln \rho, & \rho \ge 1. \end{cases}$$

The biophysical derivation of (1.3) can be found in [24]. It is worth mentioning that other forms of state equations, such as  $\Sigma(\rho) = \rho^m$ , have been proposed and studied as well [21, 22]. Letting H denote the Heaviside function, i.e., H(v) = 0 for v < 0 and H(v) = 1 for v > 0, the growth term is chosen to be

(1.4) 
$$\Phi(\rho) = \rho H(C_p - \Sigma(\rho)).$$

This indicates that when the pressure is less than a threshold denoted by  $C_p$ , i.e.,  $\Sigma(\rho) < C_p$ , the cell density grows exponentially, while the cell division stops when the process exceeds the threshold,  $\Sigma(\rho) > C_p$ . Though the state equation in (1.3) and the growth function (1.4) are not yet experimentally verified, they are qualitatively reasonable and allow for analytical formulations of the front speed.

Similar to [21, 22, 23, 24], the fluid mechanical model (1.1) (1.2) relates to a free boundary model in the incompressible limit  $(C_{\nu} \to \infty)$ . The derivation of the corresponding free boundary model from (1.1) can be seen in a heuristic way as follows. Multiplying (1.1) by  $\Sigma' = \frac{C_{\nu}}{\rho}$  in the support of  $\Sigma$ , we get

(1.5) 
$$\frac{\partial}{\partial t} \Sigma - C_S \nabla \Sigma \cdot \nabla W - C_S C_\nu \Delta W = C_\nu H.$$

Formally, sending  $C_{\nu} \to \infty$  yields the relation  $-C_S \Delta W = H$  within the support of  $\Sigma$ . Thus, in the incompressible limit, we obtain the complementary relation

(1.6) 
$$\Sigma = 0 \quad \text{or} \quad -C_S \Delta W = H.$$

Formally, one sees from (1.5) that if the initial density is compactly supported, then it remains compactly supported with boundary moving with velocity  $v = -C_S \nabla W$ , and this completes (1.6), the free boundary model. In a similar model, such a limit was proved rigorously [23].

This free boundary model has been comprehensively studied in [24] by explicitly constructing the 1D traveling wave solutions, which implies constant propagation speed of the tumor borders. However, in principle, the one-dimensional (1D) traveling wave solution is relevant only when the tumor radius is approaching infinity, and therefore it is unable to quantify the dynamics for finite size tumors. It is worth mentioning that the traveling wave solutions are also available for some multispecies models (see, e.g., [19]), which sheds light on the understanding of the tumor boundary instability.

In this paper, we construct closed-form radially symmetric solutions of the free boundary model in various dimensions. The derivation follows techniques similar to those in [17], but to the best of our knowledge, the results with exact quantification of the pressure jumps are obtained for the first time. In addition, the expressions provide strong evidence for the conjecture that the pressure jump relates to the tumor border curvature. We further carry out asymptotic analysis of the closed-form solutions in the large tumor radius regime and are able to identify the traveling wave solutions in the large radius limit. Besides, the asymptotic analysis manifests the effect of the dimension in the large radius limit. We show that in contrast to the exponential convergence of the speed toward the limit in one dimension, the convergence rate in multidimensional cases is at most algebraic.

For the cell density model, direct analysis of the boundary moving speed still seems inaccessible at this stage. Instead, we provide some a priori analysis and propose

a novel numerical scheme to simulate its dynamics. The numerical method is an improved version of our previous work [18], wherein only the Darcy's law is considered. When  $C_{\nu}$  is large, though we could only show at a formal level the convergence of the cell density model to the free boundary model, the numerical results show that the boundary moving speed and pressure jump across the tumor borders agree well with the analytical results from the free boundary model.

The rest of the paper is outlined as follows. We give an a priori  $L^2$  estimate for the fluid mechanical model in section 2, and then in section 3, based on the limiting free boundary model, we derive explicitly the velocity and structure of the tumor boundary for 1D symmetric, 2D radial symmetric, and 3D spherical symmetric cases. A new numerical scheme that captures the correct border velocity for a wide range of  $C_{\nu}$  is proposed in section 4, and in section 5 we carry out extensive numerical tests to exemplify the analytical observations.

2. A priori analysis of the cell density model. In this section, we aim to derive some a priori estimates of the cell density model. Note that although quantifying the boundary propagation speed at this level seems unreachable, the stability results we obtain below give access to the design of reliable numerical schemes. For simplicity, we assume hereinafter all the boundary terms vanish when carrying out integration by parts due to the decaying property of the solutions at infinity.

For convenience, we recall that

(2.1) 
$$\frac{\partial}{\partial t}\rho - C_S \nabla \cdot (\rho \nabla W) = \rho H(C_p - \Sigma), \qquad \mathbf{x} \in \mathbb{R}^n, \quad t \in \mathbb{R}^+,$$

$$(2.2) -C_z \Delta W + W = \Sigma, \boldsymbol{x} \in \mathbb{R}^n.$$

For simplicity of analysis, we assume that  $\forall t \geq 0$ , we have  $\Sigma(\boldsymbol{x},t)$  is continuous in  $\boldsymbol{x} \in \mathbb{R}^n$ , and  $0 \leq \Sigma(\boldsymbol{x},t) \leq C_p$ . Thus, by the maximum principle, we also have  $0 \leq W(\boldsymbol{x},t) \leq C_p$ , and from (2.2), it implies  $\Delta W \in \left[-\frac{C_p}{C_z}, \frac{C_p}{C_z}\right]$ . Note that  $\Delta W$  may change signs in the whole space.

Next, we check the  $L^2$  stability of the density  $\rho$ . Assuming  $\rho(\boldsymbol{x},0)$  is compactly supported and  $\|\rho(\cdot,0)\|_{L^2}$  is finite, multiplying (2.1) by  $\rho$  and integrating over  $\mathbb{R}^n$ , we get

$$\frac{1}{2} \frac{d}{dt} \int_{\mathbb{R}^d} |\rho|^2 d\mathbf{x} = C_S \int_{\mathbb{R}^d} \rho \nabla \cdot (\rho \nabla W) d\mathbf{x} + \int_{\mathbb{R}^d} |\rho|^2 H(1 - \Sigma) d\mathbf{x} 
= \frac{C_S}{2} \int_{\mathbb{R}^n} |\rho|^2 \Delta W d\mathbf{x} + \int_{\mathbb{R}^d} |\rho|^2 H(1 - \Sigma) d\mathbf{x},$$

which implies that

$$\frac{d}{dt} \|\rho\|_{L^2}^2 \leq \left(\frac{C_S C_p}{C_z} + 2\right) \|\rho\|_{L^2}^2,$$

and therefore an upper bound for the relative growth rate of  $\|\rho\|_{L^2}$  is guaranteed.

We now analyze the  $L^2$  stability of the pressure function  $\Sigma$ . We denote by  $D(t) = \{x : \Sigma(x,t) > 0\}$  and assume that  $D(t) \in \mathbb{R}^n$  is compact, then

$$\frac{\partial}{\partial t} \Sigma - C_S \nabla \Sigma \cdot \nabla W - C_S C_\nu \Delta W = C_\nu H, \quad x \in D(t).$$

Multiply each side by  $\Sigma$  and integrate over  $\mathbb{R}^n$ , we have

$$\frac{1}{2}\frac{d}{dt}\int_{\mathbb{R}^n}|\Sigma|^2d\boldsymbol{x}-C_S\int_{\mathbb{R}^n}\Sigma\nabla\Sigma\cdot\nabla Wd\boldsymbol{x}-C_SC_\nu\int_{\mathbb{R}^n}\Sigma\Delta Wd\boldsymbol{x}=C_\nu\int_{D(t)}\Sigma Hd\boldsymbol{x}.$$

By (2.2) and the boundedness of W and  $\Delta W$  above, we get

$$\begin{split} \int_{\mathbb{R}^n} \Sigma \nabla \Sigma \cdot \nabla W d\boldsymbol{x} &= -\frac{1}{2} \int_{\mathbb{R}^n} (\Sigma)^2 \Delta W d\boldsymbol{x} \\ &= -\frac{1}{2} \int_{\mathbb{R}^n} (-C_z \Delta W + W)^2 \Delta W d\boldsymbol{x} \\ &= -\frac{1}{2} \int_{\mathbb{R}^n} \left[ (C_z)^2 |\Delta W|^2 \Delta W - 2C_z |\Delta W|^2 W + W^2 \Delta W \right] d\boldsymbol{x} \\ &= -\frac{1}{2} \int_{\mathbb{R}^n} \left[ C_z |\Delta W|^2 (C_z \Delta W - W) - C_z |\Delta W|^2 W - 2W |\nabla W|^2 \right] d\boldsymbol{x} \\ &= -\frac{1}{2} \int_{\mathbb{R}^n} \left[ -C_z |\Delta W|^2 \Sigma - C_z |\Delta W|^2 W - 2W |\nabla W|^2 \right] d\boldsymbol{x} \\ &\leq C_p C_z \int_{\mathbb{R}^n} |\Delta W|^2 d\boldsymbol{x} + C_p \int_{\mathbb{R}^n} |\nabla W|^2 d\boldsymbol{x}, \end{split}$$

and

$$\int_{\mathbb{R}^n} \Sigma \Delta W d\boldsymbol{x} = \int_{\mathbb{R}^n} (-C_z \Delta W + W) \Delta W d\boldsymbol{x} = -\int_{\mathbb{R}^n} C_z |\Delta W|^2 + |\nabla W|^2 d\boldsymbol{x}.$$

Denote V(t) = Vol(D(t)), then clearly we obtain  $C_{\nu} \int_{D(t)} \Sigma H dx \leq C_p C_{\nu} V(t)$ . Altogether, we have the following estimate:

$$(2.3) \frac{1}{2} \frac{d}{dt} \int_{\mathbb{R}^n} |\Sigma|^2 d\mathbf{x} \le C_S C_z \left( C_p - C_{\nu} \right) \int_{\mathbb{R}^n} |\Delta W|^2 d\mathbf{x} + C_S (C_p - C_{\nu}) \int_{\mathbb{R}^n} |\nabla W|^2 d\mathbf{x} + C_p C_{\nu} V(t).$$

Clearly, when  $C_{\nu} > C_p$  the diffusion dominates the convection and results in an overall stabilizing effect.

3. The free boundary model. In this section, we construct analytical solutions to the free boundary problem based on the three-zone ansatz, which was originally proposed in [24] for the construction of traveling wave solutions. However, unlike the traveling wave solution where the inner layer is infinite, here we assume that the inner layer has a finite size. We shall show that, with the specific choice of solution ansatz described below, the free boundary model reduces to a differential-algebraic system of equations, where the differential equation of the radius determines the border expansion speed and the algebraic equation governs the thicknesses of the inner and outer layers of the tumor.

We will also investigate the large radius limit when the thickness of the inner layer becomes infinity. In such limits, the radial symmetric solutions to the free boundary model always converge to a traveling wave solution, regardless of the spatial dimensions, but with different convergence rates. In multidimensions the convergence rates are algebraic with respect to the radius of the inner layer, which gives hints to the dependence of the curvature (the reciprocal of the radius in this case) in the first order correction of the front moving speed.

In the incompressible limit, we consider the Hele–Shaw type complementary equation and the Brinkman model

(3.1a) 
$$\begin{cases} \Sigma = 0 \text{ or } -C_S \Delta W = H(C_p - \Sigma), & \boldsymbol{x} \in \mathbb{R}^n. \\ -C_z \Delta W + W = \Sigma, & \boldsymbol{x} \in \mathbb{R}^n. \end{cases}$$

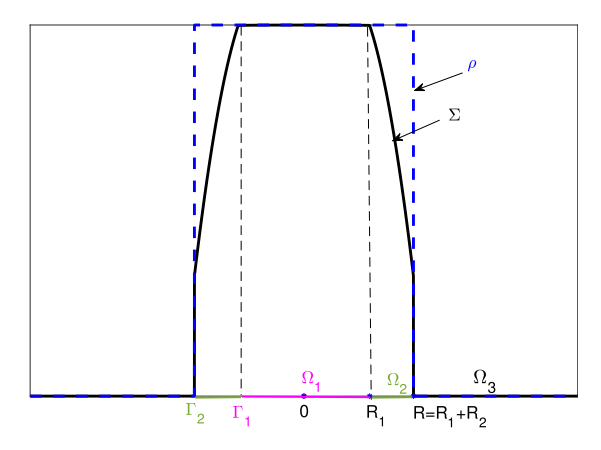


Fig. 3.1. Schematic plot of the solution ansatz. The support of the tumor consists of two layers:  $\Omega_1$  and  $\Omega_2$ , which define the inner boundary  $\Gamma_1$  and the outer boundary  $\Gamma_2$ , respectively. Note that there is a possible pressure jump across  $\Gamma_2$ .

The free boundary model is completed by the boundary moving velocity  $v = -C_S \nabla W$ . Particularly, we are interested in solutions with density  $\rho$  evolving as a characteristic function on a changing domain and pressure  $\Sigma$  may vary within the support of  $\rho$ .

To this end, we assume that the whole domain can be divided into three parts: in  $\Omega_1$ ,  $\Sigma = C_p$ ,  $\rho = 1$ , and its boundary is denoted by  $\Gamma_1$ ; in  $\Omega_2$ ,  $\Sigma \in (0, C_p)$ ,  $\rho = 1$ , its inner and outer boundary are  $\Gamma_1$  and  $\Gamma_2$  respectively, and  $\Omega_1 \cap \Omega_2 = \emptyset$ ;  $\Omega_3 = (\Omega_1 \cup \Omega_2)^c$ , where  $\Sigma = 0$ , and  $\rho = 0$ .  $\Gamma_2$  is evolving in time with the normal velocity  $-\nabla W \cdot \hat{n}$ , where n is the outer unit normal vector to  $\Gamma_2$ . Please see Figure 3.1 for an illustration.

Note specifically that the support of  $\Sigma$  may not coincide with that of  $\rho$  in general, but we are only interested in deriving the analytical solutions when they do share the same support. We also expect that W and  $\nabla W$  are continuous across both  $\Gamma_1$  and  $\Gamma_2$ , whereas pressure  $\Sigma$  remains continuous across  $\Gamma_1$  but has a jump across  $\Gamma_2$ . We also note that W is not supported in  $\Omega_1 \cup \Omega_2$ , but rather W > 0 everywhere.

Since the Heaviside function H is hard to deal with, we adopt the following regularization as in [24]:

(3.2) 
$$H_{\eta}(u) = \begin{cases} 0, & u \leq 0; \\ \frac{u}{\eta}, & 0 \leq u \leq \eta; \\ 1, & u \geq \eta, \end{cases}$$

where  $\eta \in (0, C_p)$ . As a result, the decomposition of the domain is modified accordingly. In  $\Omega_1^{\eta}$ ,  $\Sigma \in (C_p - \eta, C_p]$  and  $\rho = 1$ ; in  $\Omega_2^{\eta}$ ,  $\Sigma \in (0, C_p - \eta)$  and  $\rho = 1$ ; finally in  $\Omega_3^{\eta}$ ,  $\Sigma = 0$  and  $\rho = 0$ . The continuity of W,  $\nabla W$ , and  $\Sigma$  through the boundaries  $\Gamma_1^{\eta}$  and  $\Gamma_2^{\eta}$  stays unchanged. It is expected that the regularized solution converges to the original one in the limit  $\eta \to 0^+$ .

In the rest of the section, we derive explicit solutions to the incompressible limit model using the above ansatz in various dimensions. We also investigate the solvability conditions, in order for the ansatz to be valid, and its connection to the traveling wave solution.

**3.1. 1D case.** We start with the regularized problem. For simplicity, we assume the problem is symmetric in space and denote  $\Omega_1^{\eta} = [-R_1^{\eta}(t), R_1^{\eta}(t)], \Omega_1^{\eta} \cup \Omega_2^{\eta} = [-R^{\eta}(t), R^{\eta}(t)]$  with  $R^{\eta}(0) = R_0$  being the initial condition. We first derive the equation that links  $R^{\eta}$  and  $R_1^{\eta}$ , and then the evolution equation for  $R^{\eta}$ .

In  $\Omega_1^{\eta}$ , (3.1) along with (3.2) reads

$$-C_S W_{xx} = \frac{C_p - \Sigma}{\eta}, \qquad -C_z W_{xx} + W = \Sigma \,, \label{eq:controller}$$

which readily leads to

$$-(\eta C_S + C_z)W_{xx} + W = C_p,$$

after eliminating  $\Sigma$ . Note from the symmetric assumption that W'(0) = 0, the general solution of W in  $\Omega_1^{\eta}$  is given by

$$W(x) = C_p + A^{\eta} \cosh\left(\frac{x}{\sqrt{\eta C_S + C_z}}\right), \quad x \in \Omega_1^{\eta}.$$

Consequently, the general solution of  $\Sigma$  in  $\Omega_1^{\eta}$  is given by

$$\Sigma = -C_z W_{xx} + W = C_p + \frac{A^{\eta} \eta C_S}{\eta C_S + C_z} \cosh\left(\frac{x}{\sqrt{\eta C_S + C_z}}\right), \quad x \in \Omega_1^{\eta}.$$

Since  $\Sigma$  equals  $C_p - \eta$  at the boundary of  $\Omega_1^{\eta}$ , i.e.,  $\Sigma(R_1^{\eta}) = C_p - \eta$ , we have

(3.3) 
$$A^{\eta} = -\frac{\eta C_S + C_z}{C_S \cosh\left(\frac{R_1^{\eta}}{\sqrt{\eta C_S + C_z}}\right)}.$$

In  $\Omega_2^{\eta}$ , the model (3.1) becomes

$$-C_S W_{xx} = 1, \qquad -C_z W_{xx} + W = \Sigma,$$

and one can immediately write down the general solution for W as

$$W(x) = -\frac{1}{2C_S}x^2 + a^{\eta}x + b^{\eta}, \qquad x \in \Omega_2^{\eta}.$$

By continuity of W and  $W_x$  at  $x = R_1^{\eta}$ , we get

(3.4) 
$$a^{\eta} = \frac{R_1^{\eta}}{C_S} - \frac{\sqrt{\eta C_S + C_z}}{C_S} \tanh\left(\frac{R_1^{\eta}}{\sqrt{\eta C_S + C_z}}\right),$$

(3.5) 
$$b^{\eta} = C_p - \eta - \frac{C_z}{C_S} - \frac{(R_1^{\eta})^2}{2C_S} + R_1^{\eta} \frac{\sqrt{\eta C_S + C_z}}{C_S} \tanh\left(\frac{R_1^{\eta}}{\sqrt{\eta C_S + C_z}}\right).$$

And the general solution of  $\Sigma$  in  $\Omega_2^{\eta}$  is given by

$$\Sigma(x) = -C_z W_{xx} + W = -\frac{1}{2C_S} x^2 + a^{\eta} x + b^{\eta} + \frac{C_z}{C_S}.$$

Finally, in  $\Omega_3^{\eta}$ , (3.1) simplifies to

$$\Sigma = 0, \qquad -C_z W_{xx} + W = \Sigma.$$

By assuming the decaying behavior of W at infinity, the general solution of W in  $\Omega_3^{\eta}$  can be written as

$$W(x) = d^{\eta} e^{-\frac{x - R^{\eta}}{\sqrt{C_z}}}, \qquad x \in \Omega_3^h.$$

Then the continuity of W at  $R^{\eta}$  implies

(3.6) 
$$d^{\eta} = -\frac{1}{2C_S} (R^{\eta})^2 + a^{\eta} R^{\eta} + b^{\eta}.$$

To summarize, we have the following analytical representation of  $\Sigma$  and W in different domains:

(3.7) 
$$W(x) = \begin{cases} C_p + A^{\eta} \cosh\left(\frac{x}{\sqrt{\eta C_S + C_z}}\right), & x \in \Omega_1^{\eta}, \\ -\frac{1}{2C_S} x^2 + a^{\eta} x + b^{\eta}, & x \in \Omega_2^{\eta}, \\ d^{\eta} e^{-\frac{x - R^{\eta}}{\sqrt{C_z}}}, & x \in \Omega_3^{\eta}. \end{cases}$$

(3.8) 
$$\Sigma(x) = \begin{cases} C_p + \frac{A^{\eta} \eta C_S}{\eta C_S + C_z} \cosh\left(\frac{x}{\sqrt{\eta C_S + C_z}}\right), & x \in \Omega_1^{\eta}, \\ -\frac{1}{2C_S} x^2 + a^{\eta} x + b^{\eta} + \frac{C_z}{C_S}, & x \in \Omega_2^{\eta}, \\ 0, & x \in \Omega_3^{\eta}, \end{cases}$$

where  $a^{\eta}$ ,  $b^{\eta}$ ,  $d^{\eta}$ , and  $A^{\eta}$  are given by (3.4), (3.5), (3.6), and (3.3), respectively.

Thus, the regularized problem has been completely solved. We take the limit  $\eta \to 0$ , and the solution becomes

(3.9) 
$$W(x) = \begin{cases} C_p + A \cosh\left(\frac{x}{\sqrt{C_z}}\right), & x \in \Omega_1, \\ -\frac{1}{2C_S}x^2 + ax + b, & x \in \Omega_2, \\ de^{-\frac{x-R}{\sqrt{C_z}}}, & x \in \Omega_3; \end{cases}$$

(3.10) 
$$\Sigma(x) = \begin{cases} C_p, & x \in \Omega_1, \\ -\frac{1}{2C_S}x^2 + ax + b + \frac{C_z}{C_S}, & x \in \Omega_2, \\ 0, & x \in \Omega_3, \end{cases}$$

where the parameters are listed below:

$$\begin{split} a &= \frac{R_1}{C_S} - \frac{\sqrt{C_z}}{C_S} \tanh\left(\frac{R_1}{\sqrt{C_z}}\right), \quad b = C_p - \frac{C_z}{C_S} - \frac{(R_1)^2}{2C_S} + R_1 \frac{\sqrt{C_z}}{C_S} \tanh\left(\frac{R_1}{\sqrt{C_z}}\right), \\ A &= -\frac{C_z}{C_S \cosh\left(\frac{R_1}{\sqrt{C_z}}\right)}, \qquad d = -\frac{1}{2C_S} (R)^2 + aR + b \,. \end{split}$$

Next, we examine the relationship between two boundaries R and  $R_1$ . Again by continuity of  $W_x$  at R, one has

$$-\frac{R}{C_S} + a = -\frac{d}{\sqrt{C_z}}.$$

If we denote the difference between those two by  $R_2$ , namely  $R = R_1 + R_2$ , then (3.11) becomes

$$\frac{\sqrt{C_z}}{C_S}R_2 + \frac{C_z}{C_S}\tanh\left(\frac{R_1}{\sqrt{C_z}}\right) = -\frac{1}{2C_S}(R_2)^2 - R_2\frac{\sqrt{C_z}}{C_S}\tanh\left(\frac{R_1}{\sqrt{C_z}}\right) + C_p - \frac{C_z}{C_S},$$

which simplifies to a quadratic equation in  $R_2$ ,

(3.12)

$$(R_2)^2 + 2\sqrt{C_z} \left( 1 + \tanh\left(\frac{R_1}{\sqrt{C_z}}\right) \right) R_2 + 2C_z \left( 1 + \tanh\left(\frac{R_1}{\sqrt{C_z}}\right) \right) - 2C_p C_S = 0.$$

We remark that, given the parameters  $C_p$ ,  $C_z$ , and  $C_S$  (note that  $C_{\nu} \to \infty$ ), the necessary condition for the above solution to make sense is that  $R \geq R_1 \geq 0$ . This implies that, in the algebraic equation (3.12), given the value for the outer boundary,  $R = R_1 + R_2$ , there exist solutions with  $R_1 \geq 0$  and  $R_2 \geq 0$ . Although one cannot get explicit constraints from such solvability conditions, it is easy check the condition numerically; see Figure 3.2 on the left. The other two plots in Figure 3.2 indicate that if we choose R and  $R_1$  satisfying the relation (3.12), then W has a smooth transition from  $\Omega_1$  to  $\Omega_2$  (middle plot), and a kink otherwise (right plot).

To make a connection to the traveling wave solutions, we consider the limit  $R_1 \to \infty$ . Then (3.12) reduces to

$$(R_2)^2 + 4\sqrt{C_z}R_2 + 4C_z - 2C_pC_S = 0,$$

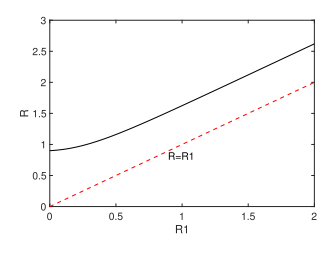
which has the following two solutions:  $R_2 = \pm \sqrt{2C_pC_S} - 2\sqrt{C_z}$ . Therefore, when  $\sqrt{2C_pC_S} > 2\sqrt{C_z}$ ,  $R_2$  has a positive solution, which means in the traveling wave limit, i.e.,  $R_1 \to \infty$ ,  $\Omega_2$  persists with width  $\sqrt{2C_pC_S} - 2\sqrt{C_z}$ .

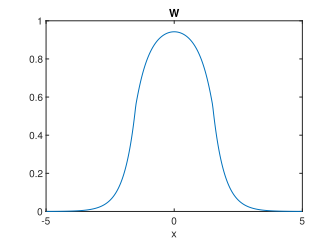
In this case, we can further calculate the pressure jump at R, which is given by  $\Sigma(R) = d + \frac{C_z}{C_S}$ . With (3.11), it becomes

$$\Sigma(R) = \frac{\sqrt{C_z}}{C_S} R_2 + \frac{\sqrt{C_z} \sqrt{C_z}}{C_S} \tanh\left(\frac{R_1}{\sqrt{C_z}}\right) + \frac{C_z}{C_S}.$$

If we take  $R_1 \to \infty$ , the pressure at  $\Gamma_2$  simplifies to

$$\Sigma(R) = \frac{\sqrt{C_z}}{C_S} R_2 + 2\frac{C_z}{C_S}.$$





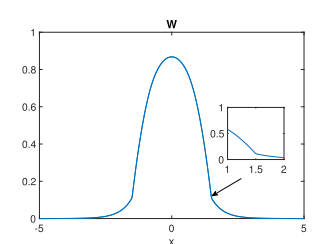


FIG. 3.2. Left: relationship between  $R_1$  and R. Middle: plot of W(x) using (3.9) with R=1.5 and  $R_1=1.2781$ , satisfying the relation (3.12). Right: plot of W(x) using (3.9) with R=1.5 and  $R_1=0.8$ , not satisfying the relation (3.12). Here  $C_S=1$ ,  $C_z=2$ ,  $C_p=4$ ,  $C_\nu=200$ ,  $\eta=0.001$ .

When  $\sqrt{2C_pC_S} > 2\sqrt{C_z}$ , we substitute  $R_2$  with  $\sqrt{2C_pC_S} - 2\sqrt{C_z}$  and get the pressure jump

$$\Sigma(R) = \sqrt{\frac{2C_zC_p}{C_S}}.$$

This recovers traveling wave solutions found in [24].

When  $R_1$  is finite, there is no explicit analytical solution; instead we numerically solve (3.12) for  $R_1$ . Here R(t) satisfies

$$\begin{split} \dot{R} &= -C_S W_x(R) = R - C_S \left( \frac{R_1}{C_S} - \frac{\sqrt{C_z}}{C_S} \tanh \left( \frac{R_1}{\sqrt{C_z}} \right) \right) \\ &= R - R_1 + \sqrt{C_z} \tanh \left( \frac{R_1}{\sqrt{C_z}} \right). \end{split}$$

When  $\sqrt{2C_pC_S} > 2\sqrt{C_z}$ , in the traveling wave limit,  $R_1 \to \infty$ , we obtain

$$\dot{R} = \sqrt{2C_p C_S} - \sqrt{C_z}.$$

**3.2. 2D radial symmetric case.** Similar to the 1D case, with the radial symmetric assumption, we can explicitly solve for the ansatz solution to the regularized impressible model. The interested readers may refer to Appendix A.1 for details. In the following,  $I_m(r)$  denotes the modified Bessel function of the first kind, and  $K_m(r)$  denotes the modified Bessel function of the second kind. By taking the limit  $\eta \to 0$ , we obtain the solution to the incompressible limit model

(3.13) 
$$W(r) = \begin{cases} C_p + AI_0\left(\frac{r}{\sqrt{C_z}}\right), & r \in \Omega_1 \\ -\frac{1}{4C_S}r^2 + a\ln r + b, & r \in \Omega_2, \\ dK_0\left(\frac{r}{\sqrt{C_z}}\right), & r \in \Omega_3, \end{cases}$$

(3.14) 
$$\Sigma(r) = \begin{cases} C_p, & r \in \Omega_1, \\ -\frac{1}{4C_S}r^2 + a\ln r + b + \frac{C_z}{C_S}, & r \in \Omega_2, \\ 0, & r \in \Omega_3, \end{cases}$$

where the parameters are listed below:

$$\begin{split} a &= \frac{1}{2C_S} R_1^2 - R_1 \frac{\sqrt{C_z}}{C_S} \frac{I_1\left(\frac{R_1}{\sqrt{C_z}}\right)}{I_0\left(\frac{R_1}{\sqrt{C_z}}\right)}, \\ b &= C_p - \frac{C_z}{C_S} + \frac{(R_1)^2}{4C_S} - \frac{(R_1)^2 \ln R_1}{2C_S} + R_1 \ln R_1 \frac{\sqrt{C_z}}{C_S} \frac{I_1\left(\frac{R_1}{\sqrt{C_z}}\right)}{I_0\left(\frac{R_1}{\sqrt{C_z}}\right)}, \\ A &= -\frac{C_z}{C_S I_0\left(\frac{R_1}{\sqrt{C_z}}\right)}, \qquad dK_0\left(\frac{R}{\sqrt{C_z}}\right) = -\frac{1}{4C_S} R^2 + a \ln R + b \,. \end{split}$$

Next, we examine the relationship between two boundaries R and  $R_1$ . Again by continuity of  $W_r$  at R, one has

$$-\frac{d}{\sqrt{C_z}}K_1\left(\frac{R}{\sqrt{C_z}}\right) = -\frac{1}{2C_S}R + \frac{a}{R}.$$

If we denote the difference between those two by  $R_2$ , namely  $R = R_1 + R_2$ , then

(3.15) 
$$\sqrt{C_z} \frac{K_0\left(\frac{R}{\sqrt{C_z}}\right)}{K_1\left(\frac{R}{\sqrt{C_z}}\right)} \left(\frac{1}{2C_S}R - \frac{a}{R}\right) = -\frac{1}{4C_S}R^2 + a\ln R + b.$$

To see the connection to the traveling wave model, we consider the case with  $R_1 \gg 1$ ,  $R_2 = O(1)$ . Asymptotically expanding (3.15), we get

L.H.S.

$$\begin{split} &=\sqrt{C_z}\left(1-\frac{\sqrt{C_z}}{2R}\right)\left(\frac{1}{C_S}R_2+\frac{\sqrt{C_z}}{C_S}\frac{I_1\left(\frac{R_1}{\sqrt{C_z}}\right)}{I_0\left(\frac{R_1}{\sqrt{C_z}}\right)}+\frac{1}{R_1}\left(\frac{R_2^2}{2C_S}-R_2\frac{\sqrt{C_z}}{C_S}\frac{I_1\left(\frac{R_1}{\sqrt{C_z}}\right)}{I_0\left(\frac{R_1}{\sqrt{C_z}}\right)}\right)\right)\\ &+o\left(\frac{1}{R_1}\right)\\ &=\sqrt{C_z}\left(1-\frac{\sqrt{C_z}}{2R_1}\right)\left(\frac{1}{C_S}R_2+\frac{\sqrt{C_z}}{C_S}+\frac{1}{R_1}\left(\frac{R_2^2}{2C_S}-R_2\frac{\sqrt{C_z}}{C_S}-\frac{C_z}{2C_S}\right)\right)+o\left(\frac{1}{R_1}\right). \end{split}$$

Here, we have used the fact that when  $z \gg 1$ 

$$\frac{I_1(z)}{I_0(z)} = 1 - \frac{1}{2z} + o\left(\frac{1}{z}\right), \quad \frac{K_0(z)}{K_1(z)} = 1 - \frac{1}{2z} + o\left(\frac{1}{z}\right).$$

Similarly, on the right-hand side, we have

R.H.S.

$$\begin{split} &= -\frac{1}{2C_S}R_2^2 - R_2\frac{\sqrt{C_z}}{C_S}\frac{I_1\left(\frac{R_1}{\sqrt{C_z}}\right)}{I_0\left(\frac{R_1}{\sqrt{C_z}}\right)} + C_p - \frac{C_z}{C_S} + \frac{1}{R_1}\left(\frac{R_2^3}{6C_S} + \frac{R_2^2}{2}\frac{\sqrt{C_z}}{C_S}\frac{I_1\left(\frac{R_1}{\sqrt{C_z}}\right)}{I_0\left(\frac{R_1}{\sqrt{C_z}}\right)}\right) \\ &+ o\left(\frac{1}{R_1}\right) \\ &= -\frac{1}{2C_S}R_2^2 - R_2\frac{\sqrt{C_z}}{C_S} + C_p - \frac{C_z}{C_S} + \frac{1}{R_1}\left(\frac{R_2^3}{6C_S} + \frac{R_2^2}{2}\frac{\sqrt{C_z}}{C_S} + \frac{R_2C_z}{2C_S}\right) + o\left(\frac{1}{R_1}\right). \end{split}$$

To match the terms by order, we assume that when  $R_1 \gg 1$ ,

$$R_2 = \alpha_0 + \frac{\alpha_1}{R_1} + o\left(\frac{1}{R_1}\right).$$

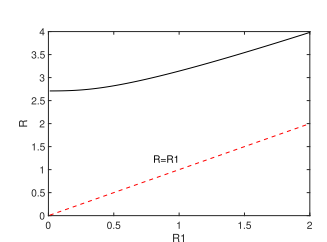
Then to the leading order, we have

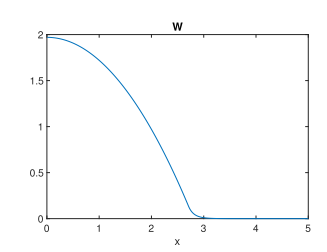
$$(\alpha_0)^2 + 4\sqrt{C_z}\alpha_0 + 4C_z - 2C_pC_S = 0$$

which implies  $\alpha_0^{\pm} = \pm \sqrt{2C_pC_S} - 2\sqrt{C_z}$ .  $\alpha_1$  is determined via the next order equation. If we consider the traveling wave limit, namely  $R_1 \to \infty$ , then clearly  $R_2 \to \alpha_0$  with an algebraic convergence rate. And if  $\alpha_0^+ > 0$ , or equivalently  $C_pC_S > 2C_z$ , then  $\Omega_2$  persists with width  $\alpha_0^+$ .

The pressure at  $\Gamma_2$  in the limit  $R_1 \to \infty$  simplifies to  $\Sigma(R) = \frac{\sqrt{C_z}}{C_S} R_2 + 2 \frac{C_z}{C_S}$ . When  $\alpha_0^+ > 0$ , substituting  $R_2$  with  $\alpha_0^+$  leads to the following pressure jump:

$$\Sigma(R) = \sqrt{\frac{2C_z C_p}{C_S}}.$$





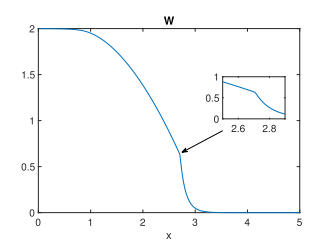


Fig. 3.3. Left: relationship between  $R_1$  and R. Middle: plot of W(x) using (3.13) with R=2.71 and  $R_1=0.0151$ , satisfying the relation (3.15). Right: plot of W(x) using (3.13) with R=2.71 and  $R_1=0.9$ , not satisfying the relation (3.15). Here  $C_S=1$ ,  $C_z=0.02$ ,  $C_p=2$ ,  $C_{\nu}=100$ ,  $\eta=0.01$ .

When  $R_1$  is finite, there is no explicit solution for  $R_2$ ; instead we consider the evolution equation for R(t)

(3.16) 
$$\dot{R} = -C_S W_r(R) = \frac{R}{2} - \frac{1}{R} \left( \frac{1}{2} (R_1)^2 - R_1 \sqrt{C_z} \frac{I_1 \left( \frac{R_1}{\sqrt{C_z}} \right)}{I_0 \left( \frac{R_1}{\sqrt{C_z}} \right)} \right).$$

Therefore, (3.16) and (3.15) can be viewed as a differential-algebraic system of equations, and we can numerically solve for  $R_1$  and R. Like before, the solvability calls for  $R \geq R_1 \geq 0$ . We display the relationship between R and  $R_1$  from (3.15) in Figure 3.3, where a monotone relation is observed.

Further, when  $\alpha_0^+ > 0$ , in the traveling wave limit  $R_1 \to \infty$ , we obtain

$$\dot{R} = \alpha_0^+ + \sqrt{C_z} = \sqrt{2C_pC_S} - \sqrt{C_z},$$

which is the same speed as we obtained in 1D case.

We want to point out that the significant difference between the 1D and 2D cases is that in two dimensions the effect of curvatures becomes manifest. Indeed, in two dimensions, when  $R_1 \gg 1$ , as the asymptotic analysis above shows, the free boundary limit converges to the traveling wave solution only with an algebraic rate. In particular, when  $R_1 \gg 1$ , we have  $R_2 \sim \alpha_0 + \kappa \alpha_1$ , where  $\kappa = 1/R$  is the curvature of the tumor front, which asymptotically determines the first order correction of the front propagation speed and the pressure jump. On the contrary, in one dimension, the free boundary limit converges to the traveling wave limit exponentially.

**3.3. 3D** spherical symmetric case. Similar to the 1D case, with the radial symmetric assumption, we can explicitly solve for the ansatz solution to the regularized impressible model. Here we only list the results, and interested readers can refer to Appendix A.2 for details. In the following,  $i_m(r)$  denotes the modified spherical Bessel function of the first kind and  $k_m(r)$  denotes the modified spherical Bessel function of the second kind. The solution to the incompressible limit model takes the following form:

$$W(r) = \begin{cases} C_p + A i_0 \left(\frac{r}{\sqrt{C_z}}\right), & r \in \Omega_1, \\ -\frac{1}{6C_S} r^2 + a \frac{1}{r} + b, & r \in \Omega_2, \\ dk_0 \left(\frac{r}{\sqrt{C_z}}\right), & r \in \Omega_3, \end{cases} \qquad \Sigma(r) = \begin{cases} C_p, & r \in \Omega_1, \\ -\frac{1}{6C_S} r^2 + a \frac{1}{r} + b + \frac{C_z}{C_S}, & r \in \Omega_2, \\ 0, & r \in \Omega_3, \end{cases}$$

where the parameters are listed below:

$$a = -\frac{1}{3C_S}(R_1)^3 + (R_1)^2 \frac{\sqrt{C_z}}{C_S} \frac{i_1\left(\frac{R_1}{\sqrt{C_z}}\right)}{i_0\left(\frac{R_1}{\sqrt{C_z}}\right)}, \quad b = C_p - \frac{C_z}{C_S} + \frac{(R_1)^2}{2C_S} - R_1 \frac{\sqrt{C_z}}{C_S} \frac{i_1\left(\frac{R_1}{\sqrt{C_z}}\right)}{i_0\left(\frac{R_1}{\sqrt{C_z}}\right)},$$

$$A = -\frac{C_z}{C_S i_0\left(\frac{R_1}{\sqrt{C_z}}\right)}, \quad dk_0\left(\frac{R}{\sqrt{C_z}}\right) = -\frac{1}{6C_S}R^2 + a\frac{1}{R} + b.$$

To get the relationship between two boundaries R and  $R_1$ , again by continuity of  $W_r$  at R, one has

$$(3.17) -\frac{d}{\sqrt{C_z}}k_1\left(\frac{R}{\sqrt{C_z}}\right) = -\frac{1}{3C_S}R - \frac{a}{R^2}.$$

Using  $R = R_1 + R_2$ , it becomes

(3.18) 
$$\sqrt{C_z} \frac{k_0 \left(\frac{R}{\sqrt{C_z}}\right)}{k_1 \left(\frac{R}{\sqrt{C_z}}\right)} \left(\frac{1}{3C_S} R + \frac{a}{R^2}\right) = -\frac{1}{6C_S} R^2 + a\frac{1}{R} + b.$$

Now we consider the case when

$$R_1 \gg 1$$
,  $R_2 = O(1)$ .

By asymptotically expanding each side of (3.18), we get

L.H.S. = 
$$\sqrt{C_z} \left( 1 - \frac{\sqrt{C_z}}{R_1} \right) \left( \frac{1}{C_S} R_2 + \frac{\sqrt{C_z}}{C_S} + \frac{1}{R_1} \left( -\frac{R_2^2}{C_S} - R_2 \frac{2\sqrt{C_z}}{C_S} - \frac{C_z}{C_S} \right) \right) + o\left( \frac{1}{R_1} \right).$$

Here, we have used the fact that when  $z \gg 1$ 

$$\frac{i_1(z)}{i_0(z)} = 1 - \frac{1}{z} + o\left(\frac{1}{z}\right), \quad \frac{k_0(z)}{k_1(z)} = 1 - \frac{1}{z} + o\left(\frac{1}{z}\right).$$

Similarly, on the right-hand side, we have

$$\text{R.H.S.} = -\frac{1}{2C_S}R_2^2 - R_2\frac{\sqrt{C_z}}{C_S} + C_p - \frac{C_z}{C_S} + \frac{1}{R_1}\left(\frac{R_2^3}{3C_S} + R_2^2\frac{\sqrt{C_z}}{C_S} + \frac{R_2C_z}{C_S}\right) + o\left(\frac{1}{R_1}\right).$$

To match the terms order by order, we assume when  $R_1 \gg 1$ ,

$$R_2 = \alpha_0 + \frac{\alpha_1}{R_1} + o\left(\frac{1}{R_1}\right) ;$$

then the leading order terms read

$$(\alpha_0)^2 + 4\sqrt{C_z}\alpha_0 + 4C_z - 2C_pC_S = 0,$$

which implies  $\alpha_0^{\pm} = \pm \sqrt{2C_pC_S} - 2\sqrt{C_z}$ .

In the traveling wave limit, namely  $R_1 \to \infty$ , then clearly  $R_2 \to \alpha_0$  with an algebraic convergence rate. If further  $\alpha_0^+ > 0$ , or equivalently  $C_p C_S > 2C_z$ , then  $\Omega_2$  persists with width  $\alpha_0^+$  in the limit.

As  $R_1 \to \infty$ , the pressure at  $\Gamma_2$  simplifies to  $\Sigma(R) = \frac{\sqrt{C_z}}{C_S} R_2 + 2 \frac{C_z}{C_S}$ .  $\alpha_0^+ > 0$ , we substitute  $R_2$  with  $\alpha_0^+$ , and we obtain the following pressure jump:

$$\Sigma(R) = \sqrt{\frac{2C_zC_p}{C_S}}.$$

Next, we check the front moving speed. When,  $R_1$  is finite, there is no direct explicit solution for  $R_2$ . Observe that the R(t) satisfies

(3.19) 
$$\dot{R} = -C_S W_r(R) = \frac{R}{3} + \frac{1}{R^2} \left( -\frac{1}{3} (R_1)^3 + (R_1)^2 \sqrt{C_z} \frac{i_1 \left(\frac{R_1}{\sqrt{C_z}}\right)}{i_0 \left(\frac{R_1}{\sqrt{C_z}}\right)} \right).$$

Thus, (3.19) and (3.18) can be viewed as a differential-algebraic system of equations, and we can numerically solve for  $R_1$  and R from this system. When  $\alpha_0^+ > 0$ , in the traveling wave limit,  $R_1 \to \infty$ , (3.19) reduces to

$$\dot{R} = \alpha_0^+ + \sqrt{C_z} = \sqrt{2C_p C_S} - \sqrt{C_z}.$$

4. Numerical scheme. In this section, we introduce a numerical scheme for solving the cell density model (1.1)–(1.2). Our goal is to design a scheme that works for a wide range of  $C_{\nu}$  and thus can simulate solutions to the free boundary model when  $C_{\nu} \to \infty$ .

When  $C_{\nu}$  is large, from the definition of  $\Sigma$  in (1.3), the dependence of  $\Sigma$  on  $\rho$ becomes intractable. More precisely, a small error in  $\rho$  induces a big change in  $\Sigma$ . On the other hand, to find the correct front speed numerically,  $\Sigma$  has to be accurate enough. Therefore it is not an easy task to design numerical schemes that can capture the right solution behavior when  $C_{\nu}$  is large. Other numerical methods developed for the degenerate diffusion equation [3, 7, 8, 15] only work for  $C_{\nu}$  of O(1).

Since the incompressible limit (3.1) is obtained directly from the evolution equation for pressure  $\Sigma$  (1.5), we propose a three-stage prediction-correction-projection method that gives the correct border velocity for  $C_{\nu} = O(1)$  and also for  $C_{\nu} \gg 1$ . This method is essentially inspired by [18], but the prediction-projection object is changed to the potential W. In order not to obscure the focus of the current work, we avoid numerical analysis for the method and save it for future works.

**4.1.** The semidiscrete method. In this part, we introduce the semidiscrete scheme by considering the following augmented system:

(4.1a) 
$$\begin{cases} \partial_t \rho - C_S \nabla \cdot (\rho \nabla W) = \Phi(\Sigma, \rho), \\ -C_z \Delta W + W = \Sigma, \end{cases}$$

$$(4.1b) \qquad \qquad \left( -C_z \Delta W + W = \Sigma \right),$$

$$(4.2) \partial_t \Sigma - C_S \nabla \Sigma \cdot \nabla W - C_S C_\nu \Delta W = C_\nu H,$$

where  $\Sigma$  relates to  $\rho$  through the constitution relation (1.3). Recall that (4.2) is an auxiliary equation derived from (4.1a) and (1.3). Since  $\nabla W$  is important in driving  $\rho$  forward in time, we combine (4.1b) and (4.2) to derive the following evolution equation:

(4.3) 
$$\frac{\partial}{\partial t} (W - C_z \Delta W) - C_S \nabla \Sigma \cdot \nabla W - C_S C_\nu \Delta W = C_\nu H.$$

Then our semidiscrete predictor-corrector scheme reads as follows. Given  $W^n$ ,  $\rho^n$ , and  $\Sigma^n$ , we have

(4.4a) 
$$\begin{cases} \frac{(W^* - C_z \Delta W^*) - (W^n - C_z \Delta W^n)}{\Delta t} - C_S \nabla \Sigma^n \cdot \nabla W^n \\ -C_S C_\nu \Delta W^* = C_\nu H^n , \\ \frac{\rho^{n+1} - \rho^n}{\Delta t} - C_S \nabla \cdot (\rho^n \nabla W^*) = \rho^{n+1} H^n , \\ -C_z \Delta W^{n+1} + W^{n+1} = \Sigma(\rho^{n+1}) , \end{cases}$$

where we have used

$$\Sigma^n = \Sigma(\rho^n), \quad H^n = H(C_p - \Sigma^n).$$

Notice that when  $C_{\nu} \to \infty$ , (4.4a) formally reduces to

$$-C_S \Delta W^* = H^n$$

and therefore captures the free boundary limit. The use of (4.4c) is to dynamically reinforce the constitutive relation between  $\rho$  and W, which also turns out to be important for stability purpose.

**4.2. Fully discrete scheme in one dimension.** In this part, we elucidate the spatial discretization and form a fully discrete scheme for the 1D case. The 1D version of (4.4) reduces to

(4.5a) 
$$\begin{cases} \frac{(W^* - C_z \partial_{xx} W^*) - (W^n - C_z \partial_{xx} W^n)}{\Delta t} - C_S \partial_x \Sigma^n \partial_x W^n \\ -C_S C_\nu \partial_{xx} W^* = C_\nu H^n, \\ \frac{\rho^{n+1} - \rho^n}{\Delta t} - C_S \partial_x (\rho^n \partial_x W^*) = \rho^{n+1} H^n, \\ -C_z \partial_{xx} W^{n+1} + W^{n+1} = \Sigma(\rho^{n+1}). \end{cases}$$

Then to update  $W^*$  from (4.5a), we have

$$(1 - C_z \partial_{xx} - C_S C_\nu \Delta t \partial_{xx}) W^* = W^n - C_z \partial_{xx} W^n + \Delta t C_S \partial_x \Sigma^n \partial_x W^n + \Delta t C_\nu H^n.$$

To discretize in space, let  $[-L_x, L_x]$  be our computational domain and denote  $x_j = -L_x + (j - \frac{1}{2})\Delta x$ ,  $j = 1, 2, ..., N_x$ , with  $\Delta x = 2L_x/N_x$ ; then  $\rho_j$ ,  $\Sigma_j$  and  $W_j$  approximate  $\rho(x)$ ,  $\Sigma(x)$ , and W(x) at position  $r_j$ , respectively. Then we approximate the spatial derivatives in the above equation via the central difference, i.e.,

$$(\partial_{xx}W)_j = \frac{W_{j-1} - 2W_j + W_{j+1}}{\Delta x^2}, \ (\partial_x W)_j = \frac{W_{j+1} - W_{j-1}}{2\Delta x}, \ (\partial_x \Sigma)_j = \frac{\Sigma_{j+1} - \Sigma_{j-1}}{2\Delta x},$$

and we use zero boundary condition for both  $\Sigma$  and W.

To propagate  $\rho$  in time, we use the central scheme to treat the convection term in (4.5b) [16]. More specifically, let

$$u_{j+\frac{1}{2}}^{n} = C_{S} \frac{W_{j+1}^{*} - W_{j}^{*}}{\Delta x},$$

then (4.5b) is discretized as

$$(1 + \Delta t H^{n}) \rho_{j}^{n+1} = \rho_{j}^{n} + \frac{\Delta t}{2\Delta x} \left[ u_{j+\frac{1}{2}}^{n} \left( \rho_{j}^{n,R} + \rho_{j+1}^{n,L} \right) - \left| u_{j+\frac{1}{2}}^{n} \right| \left( \rho_{j}^{n,R} - \rho_{j+1}^{n,L} \right) - u_{j-\frac{1}{2}}^{n} \left( \rho_{j-1}^{n,R} + \rho_{j}^{n,L} \right) + \left| u_{j-\frac{1}{2}}^{n} \right| \left( \rho_{j-1}^{n,R} - \rho_{j}^{n,L} \right) \right],$$

$$(4.7)$$

where

 $\rho_{j}^{n,R} = \rho_{j}^{n} + \frac{1}{2}\sigma_{j}^{n}, \quad \rho_{j}^{n,L} = \rho_{j}^{n} - \frac{1}{2}\sigma_{j}^{n},$ 

and

$$\sigma_{j}^{n} = \begin{cases} 0 & \text{if } (\rho_{j+1}^{n} - \rho_{j}^{n}) (\rho_{j}^{n} - \rho_{j-1}^{n}) < 0, \\ \rho_{j}^{n} - \rho_{j-1}^{n} & \text{else if } |\rho_{j+1}^{n} - \rho_{j}^{n}| > |\rho_{j}^{n} - \rho_{j-1}^{n}|, \\ \rho_{j+1}^{n} - \rho_{j}^{n} & \text{else.} \end{cases}$$

We'd like to mention that the central scheme (see [16] for a broad discussion) is not the only choice here for spatial discretization. In fact, any shock capturing scheme should serve the purpose. This is because  $\rho$  will develop a sharp moving front that resembles a shock, then a shock capturing scheme will pick up this front with minimum diffusion.

**4.3. Fully discrete 2D radial symmetric case.** In the same line of (4.1), we first write down the augmented system for the 2D radial symmetric case

$$\begin{cases} \partial_t \rho - C_S \frac{1}{r} \partial_r (r \rho \partial_r W) = \Phi(\Sigma, \rho), \\ -C_z \frac{1}{r} \partial_r (r \partial_r W) + W = \Sigma, \end{cases}$$

$$\partial_t \Sigma - C_S \partial_r \Sigma \partial_r W - C_S C_\nu \frac{1}{r} \partial_r (r \partial_r W) = C_\nu H$$
,

and semidiscretize it in the same manner as in (4.5) to get

$$(4.8a) \begin{cases} \frac{\left(W^* - C_z \frac{1}{r} \partial_r(r \partial_r W^*)\right) - \left(W^n - C_z \frac{1}{r} \partial_r(r \partial_r W^n)\right)}{\Delta t} \\ -C_S \partial_r \Sigma^n \partial_r W^n - C_S C_\nu \frac{1}{r} \partial_r(r \partial_r W^*) = C_\nu H^n, \\ \frac{\rho^{n+1} - \rho^n}{\Delta t} - C_S \frac{1}{r} \partial_r(r \rho^n \partial_r W^*) = \rho^{n+1} H^n, \\ -C_z \frac{1}{r} \partial_r(r \partial_r W^{n+1}) + W^{n+1} = \Sigma(\rho^{n+1}). \end{cases}$$

To discretize in space, let  $[0, L_r]$  be our computational domain, and denote  $r_j = \frac{\Delta r}{2} + (j-1)\Delta r$ ,  $j=1,2,\ldots N_r$ , then  $\rho_j$ ,  $\Sigma_j$  and  $W_j$  approximate  $\rho(x)$ ,  $\Sigma(x)$ , and W(x) at position  $r_j$ , respectively. Then the spatial discretization for W reads as

$$\begin{split} & \left[ \frac{1}{r} \partial_r \left( r \partial_r W^{n+1} \right) \right]_j \\ & = \frac{1}{r_j} \left[ (r \partial_r W)_{j+\frac{1}{2}} - (r \partial_r W)_{j-\frac{1}{2}} \right] \frac{1}{\Delta r} \\ & = \frac{1}{r_j} \frac{1}{\Delta r^2} \left[ r_{j+\frac{1}{2}} W_{j+1} - \left( r_{j+\frac{1}{2}} + r_{j-\frac{1}{2}} \right) W_j + r_{j-\frac{1}{2}} W_{j-1} \right], \quad j = 2, \dots, N_r - 1, \end{split}$$

and the Neumann boundary condition implies

$$\begin{split} \left[ \frac{1}{r} \partial_r \left( r \partial_r W^{n+1} \right) \right]_1 &= \frac{1}{r_1} \left[ (r \partial_r W)_{\frac{3}{2}} - (r \partial_r W)_{\frac{1}{2}} \right] \frac{1}{\Delta r} = \frac{1}{r_1} \frac{r_{\frac{3}{2}}}{\Delta r^2} \left( W_2 - W_1 \right) \,, \\ \left[ \frac{1}{r} \partial_r \left( r \partial_r W^{n+1} \right) \right]_{N_r} &= \frac{1}{r_{N_r}} \left[ (r \partial_r W)_{N_r + \frac{1}{2}} - (r \partial_r W)_{N_r - \frac{1}{2}} \right] \frac{1}{\Delta r} \\ &= \frac{1}{r_N} \frac{r_{N_r - \frac{1}{2}}}{\Delta r^2} \left( W_{N_r - 1} - W_{N_r} \right) \,. \end{split}$$

Likewise

$$(\partial_r W)_j = \frac{1}{2\Delta r} (W_{j+1} - W_{j-1}), \quad j = 2, \dots, N_r - 1,$$

and

$$(\partial_r W)_1 = \frac{1}{2\Delta r}(W_2 - W_1), \quad (\partial_r W)_{N_r} = \frac{1}{2\Delta r}(W_{N_r} - W_{N_r-1}).$$

To update  $\rho$ , let  $g(t,r) = r\rho(t,r)$  and  $u = C_S \partial_r W$ , then (4.5b) is reformulated as

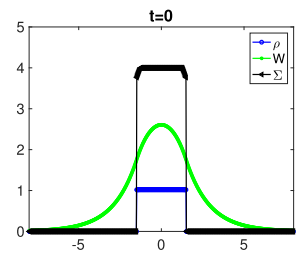
$$\frac{g^{n+1}-g^n}{\Delta t} - \partial_r(g^{n+1}u^*) = g^{n+1}H^n.$$

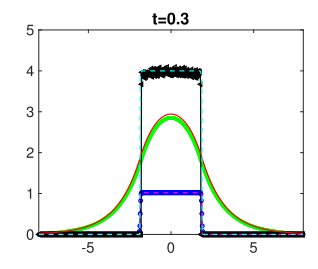
Denoting  $u_{j+\frac{1}{2}}^n = C_S \frac{W_{j+1}^* - W_j^*}{\Delta r}$ , the above equation can be discretized via the central scheme similarly as in (4.6).

5. Numerical results. In this section, we conduct a few numerical tests to explore both the model consistency and the numerical scheme's efficiency and accuracy. More specifically, we have two major objectives. First, we numerically verify that the cell density model effectively captures the incompressible limit when  $C_{\nu} \gg 1$ , and in particular, the consistences in the boundary propagation speed and in the pressure jump are carefully checked. Second, we compare the boundary moving speeds of the solutions with finite radius with those of the traveling wave solutions in one and two dimensions, respectively. We shall see the difference in the convergence trends between the 1D tests and the 2D tests, which confirms our asymptotic analysis results in section 3.

**5.1.** 1D case. First, we check the asymptotic property of the scheme (4.5) when  $C_{\nu}$  is sufficiently large. Let R(0) = 1.5, and choose  $R_2(0)$  such that it satisfies (3.12) with  $R_1(0) = R(0) - R_2(0)$ . Then, initial conditions  $\Sigma(0,x)$  and W(0,x) are chosen of the form (3.8) and (3.7), respectively, where  $\Omega_1(t) = [-R_1(0), R_1(0)]$  and  $\Omega_2 = [-R(0), -R_1(0)] \cup [R_1(0), R(0)]$ . The constants are  $C_z = 2$ ,  $C_S = 1$ ,  $C_p = 4$ ,  $C_{\nu} = 200$ . The regularization parameter  $\eta = 0.001$ . We plot the solution in Figure 5.1, where a good match between the numerical solution to model (1.1) (1.2) and the exact solution to the limit model (3.1) is observed. Here the oscillation in  $\Sigma$  is due to the amplification by log of the small oscillation in  $\rho$  near the interface.

Next, we check the behavior of the jump in  $\Sigma$ , the volume of the tumor, and the tumor invading front, versus time. The initial data is again chosen to be of the form (3.8) and (3.7) but with  $R_1 = 1$ , R = 1.5. The parameters are  $C_z = 0.2$ ,  $C_S = 1$ ,  $C_p = 1$ ,  $C_{\nu} = 50$ , and  $\eta = 0.001$ , and the results are gathered in Figure 5.2; again, good agreements between numerical solutions and theoretical predictions are observed.





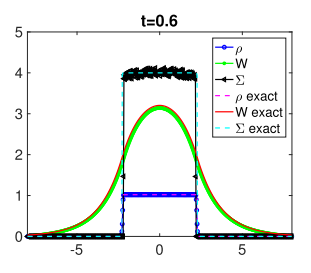


Fig. 5.1. 1D evolution of  $\rho$ ,  $\Sigma$ , and W with initial data given by the limit model. Here  $\Delta x=0.025$ ,  $\Delta t=0.0011$ . The parameters used in this example are  $C_z=2$ ,  $C_S=1$ ,  $C_p=4$ ,  $C_\nu=200$ , and  $\eta=0.001$ .

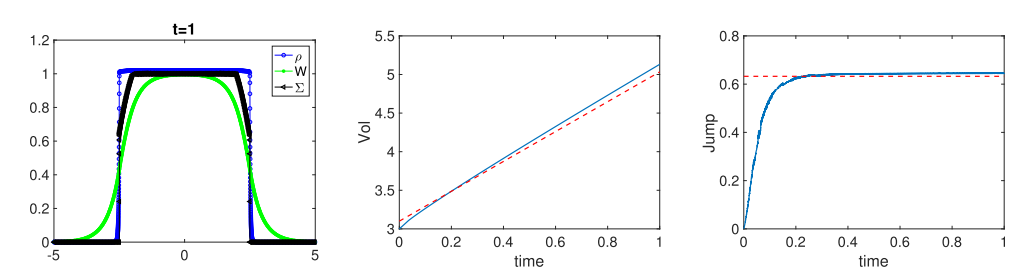


Fig. 5.2. 1D evolution of cell density model with initial data given by the limit model. Here  $\Delta x = 0.0125$ ,  $\Delta t = 9.9829e - 05$ . Left: plot of  $\rho$ ,  $\Sigma$ , and W at time t = 1. Middle: volume versus time. Here volume is  $\int \rho dx$  and the red dashed line represents slope  $2(\sqrt{2C_pC_S} - \sqrt{C_z})$  given by the analytical formula. Right: jump versus time. The red dotted line is the limit pressure jump  $\sqrt{2C_zC_p/C_S}$ .

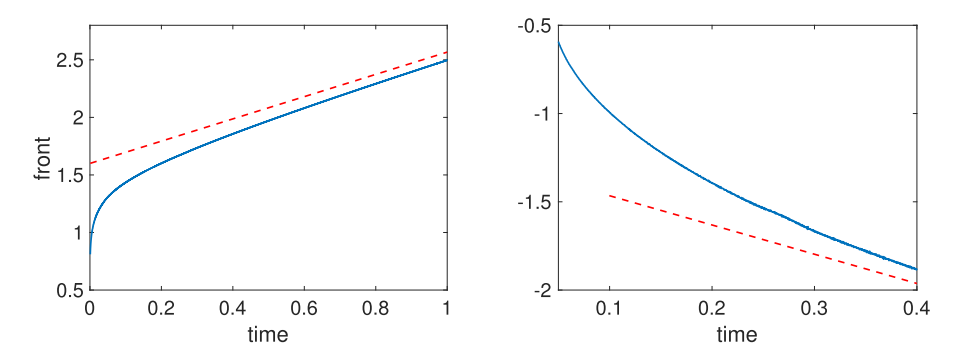


FIG. 5.3. Left: plot of the front versus time. The red dashed line indicates slope  $\sqrt{2C_pC_S} - \sqrt{C_z}$ . Right:  $\log |\dot{R}(t) - (\sqrt{2C_pC_S} - \sqrt{C_z})|$  versus time, where  $\dot{R}(t)$  denotes the front speed; the red dashed line denotes the slope  $4(\sqrt{2C_pC_S} - \sqrt{C_z})/\sqrt{C_z}$ , which is indicated by the analytical formula. Here  $\Delta x = 0.0125$ ,  $\Delta t = 9.9829e - 05$ .

We further check the convergence of propagation speed toward the limit in Figure 5.3. Here on the left, the dashed line is with slope denoted by the constant speed in the large  $R_1$  limit, corresponding to the traveling wave models. One sees that the blue curve, obtained by evolving the cell density model, approaches the red dashed line, indicating that it is the correct asymptote. On the right, an exponential convergence toward the asymptote is displayed.

**5.2. 2D radial symmetric case.** In this subsection, we consider the 2D radial symmetric case. Like before, we first check the asymptotic property of the scheme (4.8) with sufficiently large  $C_{\nu}$ . To this end, the following parameters are used:  $C_{\nu} = 50$ ,  $C_p = 1$ ,  $C_z = 0.02$ ,  $C_S = 1$ , and  $\eta = 0.01$ . Initially, let the outer radius be R(0) = 2.71, and the inner radius  $R_1(0) = 0.0151$  is obtained by solving (3.15). Then initial condition  $\Sigma(0, x)$  and W(0, x) are chosen of the form (3.14) and (3.13), respectively, where  $\Omega_1(t) = [-R_1(0), R_1(0)]$  and  $\Omega_2 = [-R(0), -R_1(0)] \cup [R_1(0), R(0)]$ . The solutions are gathered in Figure 5.4. Here a good match is observed between the numerical solution and the analytical formula.

Next, we check the jump in  $\Sigma$ , the volume of the tumor, and tumor invading front with respect to time in Figure 5.5. The initial data is again chosen to be of the form (3.8) and (3.7) but with  $R_1 = 1$ , R = 1.5. The parameters are  $C_{\nu} = 100$ ,  $C_p = 2$ ,  $C_z = 0.02$ ,  $C_S = 1$ , and  $\eta = 0.0001$ . We further check the convergence of propagation speed toward the limit in Figure 5.6. Here the major difference compared to the 1D

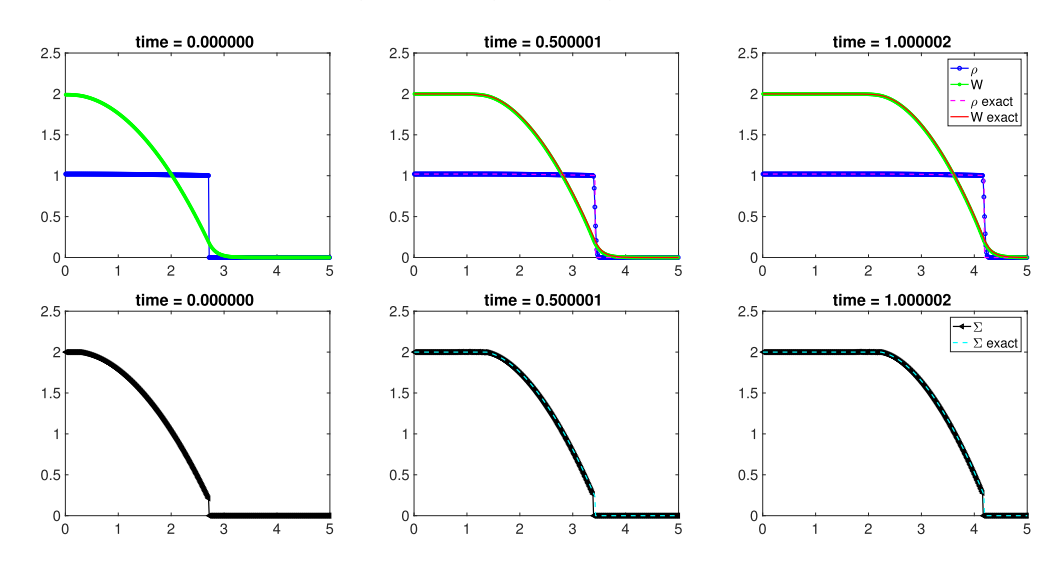


Fig. 5.4. 2D radially symmetric case. Evolution of  $\rho$ ,  $\Sigma$ , and W with initial data given by the limit model. Here  $\Delta r = 0.0125$ ,  $\Delta t = 5.3351e - 5$ . The parameters used in this example are  $C_{\nu} = 100$ ,  $C_{p} = 2$ ,  $C_{z} = 0.02$ ,  $C_{S} = 1$ , and  $\eta = 0.0001$ .

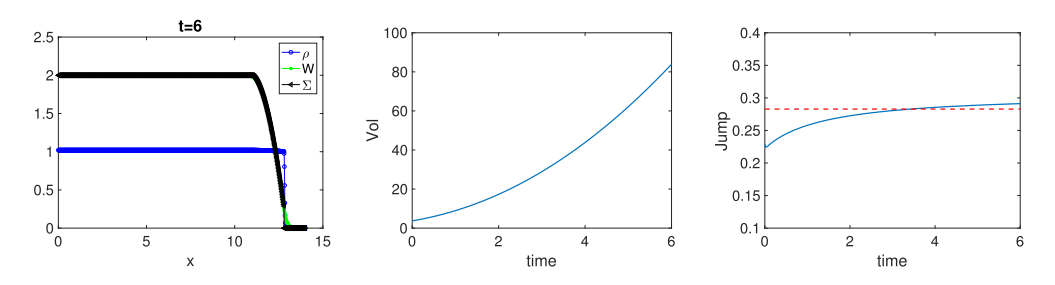


FIG. 5.5. 2D radially symmetric case with initial data given by the limit model. Here  $\Delta r = 0.0125$ ,  $\Delta t = 1.067e - 5$ . The parameters used in this example are  $C_{\nu} = 100$ ,  $C_{p} = 2$ ,  $C_{z} = 0.02$ ,  $C_{S} = 1$ , and  $\eta = 0.0001$ .

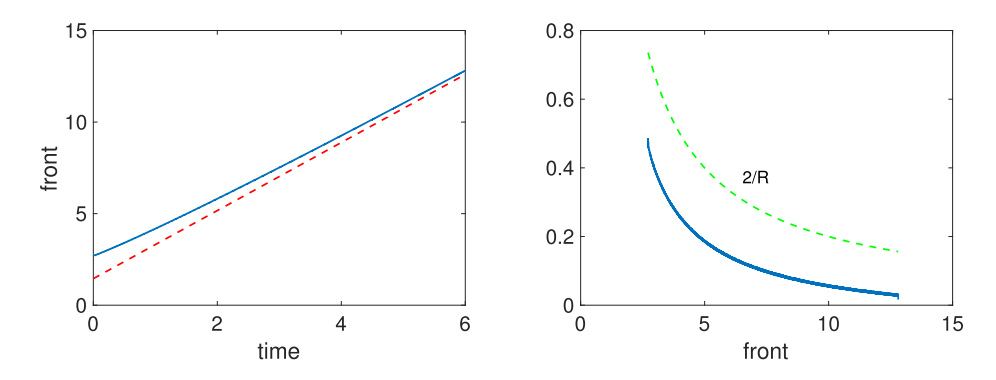


FIG. 5.6. Left: plot of the front versus time. The red dashed line represents slope  $\sqrt{2C_pC_S} - \sqrt{C_z}$ . Right: plot of  $|\dot{R}(t) - (\sqrt{2C_pC_S} - \sqrt{C_z})|$  versus front position, where  $\dot{R}(t)$  denotes the front speed. Green dashed curve denotes 2/R, where R is the front position. Here  $\Delta r = 0.0125$ ,  $\Delta t = 1.067e - 5$ . The parameters used in this example are  $C_{\nu} = 100$ ,  $C_p = 2$ ,  $C_z = 0.02$ ,  $C_S = 1$ , and  $\eta = 0.0001$ .

case is that we only observed the algebraic convergence, as can be seen on the right of the plot.

**6.** Conclusion. In this work, we explore the connections between a series of macroscopic models of tumor growth from the perspective of boundary propagation speeds. Prior to this work, only 1D traveling wave solutions have been available, which yield a constant boundary moving speed. We give reassuring justification of the results in the traveling wave model since regardless of spatial dimension, the propagation speeds of radial symmetric solutions of the free boundary model all converge to that of the 1D traveling wave model. We also offer new observation that in multidimensional cases, the convergence of the propagation speed is algebraic and the curvature of the tumor profile, which is the reciprocal of the tumor radius, shows up in the first order correction to the boundary moving speed. Between the cell density model and the free boundary model, we have numerically verified the incompressible limit, which naturally implies the convergence of the propagation speed. But still, the rigorous convergence analysis is yet to be carried out, since the previous work only applies to the tumor growth models coupled with the Darcy's law, but there should be no essential technical challenges when the Brinkman model is chosen. Besides, comprehensive numerical analysis and more general multidimensional implementation of the proposed numerical scheme are also worthy research topics. We shall pursue those directions in the future.

Appendix A. Computing the regularized incompressible model in multidimensions.

## A.1. 2D radial symmetric case. Denote

$$\Omega_1^{\eta} = B_{R_1^{\eta}(t)}, \quad \Omega_1^{\eta} \cup \Omega_2^{\eta} = B_{R^{\eta}(t)},$$

where  $B_r$  denotes a ball centered at the origin with radius r, and assume  $R^{\eta}(0) = R_0$ . Hereafter, we shall first derive the relation between  $R^{\eta}$  and  $R_1^{\eta}$ , and then the evolution equation for  $R^{\eta}$ . The derivation shares a lot in common with the 1D case, but results will have some subtle dependence on dimensions.

In  $\Omega_1^{\eta}$ , (3.1) becomes

$$-\frac{C_S}{r}(rW_r)_r = \frac{C_p - \Sigma}{\eta}, \quad -\frac{C_z}{r}(rW_r)_r + W = \Sigma,$$

which, by eliminating  $\Sigma$ , leads to

$$-(\eta C_S + C_z) \frac{1}{r} (rW_r)_r + W = C_p.$$

The symmetric assumption implies  $W_r(0) = 0$ , and therefore the general solution of W in  $\Omega_1^{\eta}$  can be written as

$$W(r) = C_p + AI_0 \left( \frac{r}{\sqrt{\eta C_S + C_z}} \right), \quad r \in \Omega_1^{\eta},$$

where  $I_m(r)$  denotes the modified Bessel function of the first kind. Thus, the general solution of  $\Sigma$  in  $\Omega_1^{\eta}$  is given by

$$\Sigma(r) = -\frac{C_z}{r}(rW_r)_r + W = C_p + \frac{A\eta C_S}{\eta C_S + C_z} I_0\left(\frac{r}{\sqrt{\eta C_S + C_z}}\right), \quad r \in \Omega_1^{\eta}.$$

Note that at the boundary  $r = R_1^{\eta}$  we have  $\Sigma(R_1^{\eta}) = C_p - \eta$ , thus

(A.1) 
$$A = -\frac{\eta C_S + C_z}{C_S I_0 \left(\frac{R_1^{\eta}}{\sqrt{\eta C_S + C_z}}\right)}.$$

In  $\Omega_2^{\eta}$ , (3.1) reads

$$-\frac{C_S}{r}(rW_r)_r = 1, \quad -\frac{C_z}{r}(rW_r)_r + W = \Sigma,$$

which immediately leads to the general solution of W

$$W(r) = -\frac{1}{4C_S}r^2 + a \ln r + b, \quad r \in \Omega_2^{\eta}.$$

By continuity of W and  $W_r$  at  $r = R_1^{\eta}$ , we get

(A.2) 
$$a^{\eta} = \frac{1}{2C_S} (R_1^{\eta})^2 - R_1^{\eta} \frac{\sqrt{\eta C_S + C_z}}{C_S} \frac{I_1 \left(\frac{R_1^{\eta}}{\sqrt{\eta C_S + C_z}}\right)}{I_0 \left(\frac{R_1^{\eta}}{\sqrt{\eta C_S + C_z}}\right)},$$

(A.3)

$$b^{\eta} = C_p - \eta - \frac{C_z}{C_S} + \frac{(R_1^{\eta})^2}{4C_S} - \frac{(R_1^{\eta})^2 \ln R_1^{\eta}}{2C_S} + R_1^{\eta} \ln R_1^{\eta} \frac{\sqrt{\eta C_S + C_z}}{C_S} \frac{I_1\left(\frac{R_1^{\eta}}{\sqrt{\eta C_S + C_z}}\right)}{I_0\left(\frac{R_1^{\eta}}{\sqrt{\eta C_S + C_z}}\right)}.$$

And the solution of  $\Sigma$  in  $\Omega_2^{\eta}$  is given by

$$\Sigma(r) = -\frac{C_z}{r}(rW_r)_r + W = -\frac{1}{4C_S}r^2 + a\ln r + b + \frac{C_z}{C_S}, \quad r \in \Omega_2^\eta \,. \label{eq:sigma}$$

Finally, in  $\Omega_3^{\eta}$ , (3.1) reduces to

$$\Sigma = 0, \quad -\frac{C_z}{r}(rW_r)_r + W = \Sigma.$$

By assuming that W decays at infinity, we have the following expression of W in  $\Omega_3^{\eta}$ :

$$W(r) = dK_0 \left(\frac{r}{\sqrt{C_z}}\right), \quad r \in \Omega_3^{\eta},$$

where  $K_m(r)$  denotes the modified Bessel function of the second kind. The continuity of both W,  $W_r$  at  $R^{\eta}$  implies

(A.4) 
$$dK_0\left(\frac{R^{\eta}}{\sqrt{C_z}}\right) = -\frac{1}{4C_S}(R^{\eta})^2 + a\ln R^{\eta} + b$$

and

$$-\frac{d}{\sqrt{C_z}}K_1\left(\frac{R^{\eta}}{\sqrt{C_z}}\right) = -\frac{1}{2C_S}R^{\eta} + \frac{a}{R^{\eta}}.$$

In summary, the analytical representation of  $\Sigma$  and W is as follows:

(A.5) 
$$W(r) = \begin{cases} C_p + AI_0 \left( \frac{r}{\sqrt{\eta C_S + C_z}} \right), & r \in \Omega_1^{\eta}, \\ -\frac{1}{4C_S} r^2 + a \ln r + b, & r \in \Omega_2^{\eta}, \\ dK_0 \left( \frac{r}{\sqrt{C_z}} \right), & r \in \Omega_3^{\eta}, \end{cases}$$

$$(A.6) \Sigma(r) = \begin{cases} C_p + \frac{A\eta C_S}{\eta C_S + C_z} I_0 \left( \frac{r}{\sqrt{\eta C_S + C_z}} \right), & r \in \Omega_1^{\eta}, \\ -\frac{1}{4C_S} r^2 + a \ln r + b + \frac{C_z}{C_S}, & r \in \Omega_2^{\eta}, \\ 0, & r \in \Omega_3^{\eta}, \end{cases}$$

where A, a, b, and d are obtained from (A.1), (A.2), (A.3), and (A.4), respectively.

**A.2. 3D spherical symmetric case.** For simplicity, we assume the problem is spherically symmetric in space, and we assume

$$\Omega_1^{\eta} = B_{R_1^{\eta}(t)}, \quad \Omega_1^{\eta} \cup \Omega_2^{\eta} = B_{R^{\eta}(t)},$$

where  $B_r$  denotes a ball centered at the origin with radius r. And we assume the initial condition

$$R^{\eta}(0) = R_0.$$

With the radial symmetric assumption, W and  $\Sigma$  are functions of only the radial variable r. The following calculations are similar to the 1D case, but we shall see some subtle effects of dimensions.

First, we aim to derive the equations that link  $R^{\eta}$  and  $R_1^{\eta}$ , and we plan to derive an evolution equation that  $R^{\eta}$  satisfies.

In  $\Omega_1^{\eta}$ , the equations are

$$-\frac{C_S}{r^2}(r^2W_r)_r = \frac{C_p - \Sigma}{\eta},$$

$$-\frac{C_z}{r^2}(r^2W_r)_r + W = \Sigma.$$

By eliminating  $\Sigma$ , we obtain

$$-(\eta C_S + C_z) \frac{1}{r^2} (r^2 W_r)_r + W = C_p.$$

The symmetric assumption implies W'(0) = 0. Therefore, the general solution of W in  $\Omega_1^{\eta}$  is given by

$$W = C_p + A i_0 \left( \frac{r}{\sqrt{\eta C_S + C_z}} \right),$$

where  $i_m(r)$  denotes the modified spherical Bessel function of the first kind. Thus, the general solution of  $\Sigma$  in  $\Omega_1^{\eta}$  is given by

$$\Sigma = -\frac{C_z}{r^2}(r^2W_r)_r + W = C_p + \frac{A\eta C_S}{\eta C_S + C_z}i_0\left(\frac{r}{\sqrt{\eta C_S + C_z}}\right).$$

The boundary condition on at  $r = R_1^{\eta}$ 

$$\Sigma(R_1^{\eta}) = C_p - \eta$$

leads to

(A.7) 
$$A = -\frac{\eta C_S + C_z}{C_S i_0 \left(\frac{R_1^{\eta}}{\sqrt{\eta C_S + C_z}}\right)}.$$

In  $\Omega_2^{\eta}$ , the equations are

$$-\frac{C_S}{r^2}(r^2W_r)_r = 1,$$
$$-\frac{C_z}{r^2}(r^2W_r)_r + W = \Sigma.$$

Obviously, the general solution of W in  $\Omega_2^{\eta}$  is given by

$$W = -\frac{1}{6C_S}r^2 + a\frac{1}{r} + b.$$

By continuity of W and  $W_r$  at  $r = R_1^{\eta}$ , we get

(A.8) 
$$a^{\eta} = -\frac{1}{3C_S} (R_1^{\eta})^3 + (R_1^{\eta})^2 \frac{\sqrt{\eta C_S + C_z}}{C_S} \frac{i_1 \left(\frac{R_1^{\eta}}{\sqrt{\eta C_S + C_z}}\right)}{i_0 \left(\frac{R_1^{\eta}}{\sqrt{\eta C_S + C_z}}\right)},$$

(A.9) 
$$b^{\eta} = C_p - \eta - \frac{C_z}{C_S} + \frac{(R_1^{\eta})^2}{2C_S} - R_1^{\eta} \frac{\sqrt{\eta C_S + C_z}}{C_S} \frac{i_1 \left(\frac{R_1^{\eta}}{\sqrt{\eta C_S + C_z}}\right)}{i_0 \left(\frac{R_1^{\eta}}{\sqrt{\eta C_S + C_z}}\right)}.$$

And the solution of  $\Sigma$  in  $\Omega_2^{\eta}$  is given by

$$\Sigma = -\frac{C_z}{r}(rW_r)_r + W = -\frac{1}{6C_S}r^2 + a\frac{1}{r} + b + \frac{C_z}{C_S}.$$

Finally, in  $\Omega_3^{\eta}$ , the equations are

$$\Sigma = 0$$

$$-\frac{C_z}{r}(rW_r)_r + W = \Sigma.$$

By assuming the decaying behavior at infinity, the general solution of W in  $\Omega_3^{\eta}$  is given by

$$W = dk_0 \left(\frac{r}{\sqrt{C_z}}\right),\,$$

where  $k_m(r)$  denotes the modified spherical Bessel function of the second kind.

The continuity of W at  $R^{\eta}$  implies

(A.10) 
$$dk_0 \left( \frac{R^{\eta}}{\sqrt{C_s}} \right) = -\frac{1}{6C_S} (R^{\eta})^2 + a \frac{1}{R^{\eta}} + b.$$

And the continuity of  $W_r$  at  $R^{\eta}$  imposes a condition between  $R_1^{\eta}$  and  $R^{\eta}$ ,

(A.11) 
$$-\frac{d}{\sqrt{C_z}}k_1\left(\frac{R^{\eta}}{\sqrt{C_z}}\right) = -\frac{1}{3C_S}R^{\eta} - \frac{a}{(R^{\eta})^2}.$$

In summary, the analytical representations of  $\Sigma$  and W are as follows:

$$(A.12) W(r) = \begin{cases} C_p + A i_0 \left(\frac{r}{\sqrt{\eta C_S + C_z}}\right), & r \in \Omega_1^{\eta}, \\ -\frac{1}{6C_S} r^2 + a \frac{1}{r} + b, & r \in \Omega_2^{\eta}, \\ dk_0 \left(\frac{r}{\sqrt{C_z}}\right), & r \in \Omega_3^{\eta}, \end{cases}$$

$$(A.13) \qquad \Sigma(r) = \begin{cases} C_p + \frac{A\eta C_S}{\eta C_S + C_z} i_0 \left(\frac{r}{\sqrt{\eta C_S + C_z}}\right), & r \in \Omega_1^{\eta}, \\ -\frac{1}{6C_S} r^2 + a \frac{1}{r} + b + \frac{C_z}{C_S}, & r \in \Omega_2^{\eta}, \\ 0, & r \in \Omega_3^{\eta}, \end{cases}$$

where A, a, b, and d are obtained from (A.7), (A.8), (A.9), and (A.10), respectively.

## REFERENCES

- D. ALEXANDER, I. KIM, AND Y. YAO, Quasi-static evolution and congested crowd transport, Nonlinearity, 27 (2014), 823.
- [2] D. Ambrosi and L. Preziosi, On the closure of mass balance models for tumor growth, Math. Models Methods Appl. Sci., 12 (2002), pp. 737–754.
- [3] T. Arbogast, M. F. Wheeler, and N. Y. Zhang, A nonlinear mixed finite element method for a degenerate parabolic equation arising in flow in porous media, SIAM J. Numer. Anal., 33 (1996), pp. 1669–1687.
- [4] N. Bellomo, N. K. Li, and P. K. Maini, On the foundations of cancer modeling: selected topics, speculations, and perspectives, Math. Models Methods Appl. Sci., 4 (2008), pp. 593-646
- [5] H. BERESTYCKI AND F. HAMEL, Reaction-Diffusion Equations and Popagation Phenomena, Springer-Verlag, New York, 2012.
- [6] R. Betteridge, M. R. Owen, H. M. Byrne, T. Alarcón, and P. K. Maini, The impact of cell crowding and active cell movement on vascular tumor growth, Netw. Heterog. Media, 1 (2006), pp. 515–535.
- [7] M. BESSEMOULIN-CHATARD AND F. FILBET, A finite volume scheme for nonlinear degenerate parabolic equations, SIAM J. Sci. Comput., 34 (2012), pp. B559–B583.
- [8] M. Burger, J. A. Carrillo, and M. T. Wolfram, A mixed finite element method for nonlinear diffusion equations, Kinet. Relat. Models, 3 (2010), pp. 59–83.
- [9] H. BYRNE AND D. DRASDO, Individual based and continuum models of growing cell populations: A comparison, J. Math. Biol., 58 (2009), pp. 657–687.
- [10] P. CIARLETTA, L. FORET, AND M. B. AMAR, The radial growth phase of malignant melanoma: multi-phase modeling, numerical simulations and linear stability analysis, J. R. Soc. Interface, 8 (2011), pp. 345–368.
- [11] K. CRAIG, I. KIM, AND Y. YAO, Congested aggregation via Newtonian interaction, Arch. Ration. Mech. Anal., 227 (2018), pp. 1–67.
- [12] E. DE ANGELIS AND L. PREZIOSI, Advection-diffusion models for solid tumour evolution in vivo and related free boundary problem, Math. Models Methods Appl. Sci., 10 (2000), pp. 379-407
- [13] A. FRIEDMAN, A Mathematical analysis and challenges arising from models of tumor growth, Math. Models Methods Appl. Sci., 17 (2007), pp. 1751–1772.

- [14] H. P. GREENSPAN, Models for the growth of a solid tumor by diffusion, Stud. Appl. Math., 51 (1972), pp. 317–340.
- [15] K. H. KARLSEN, N. H. RISEBRO, AND J. D. TOWERS, Upwind difference approximations for degenerate parabolic convection-diffusion equations with a discontinuous coefficient, IMA J. Numer. Anal., 22 (2002), pp. 623–664.
- [16] A. Kurganov and E. Tadmor, New high-resolution central schemes for nonlinear conservation laws and convection-diffusion equations, J. Comput. Phys., 160 (2000), pp. 241–282.
- [17] J.-G. LIU, M. TANG, L. WANG, AND Z. ZHOU, Analysis and computation of some tumor growth models with nutrient: From cell density models to free boundary dynamics, DCDS-B, 24 (2019), pp. 3011–3035.
- [18] J.-G. LIU, M. TANG, L. WANG, AND Z. ZHOU, An accurate front capturing scheme for tumor growth models with a free boundary limit, J. Comput. Phys., 364 (2018), pp. 73–94.
- [19] T. LORENZI, A. LORZ, AND B. PERTHAME, On interfaces between cell populations with different mobilities, Kinet. Relat. Models, 10 (2017), pp. 299–311.
- [20] B. Perthame, Some Mathematical Models of Tumor Growth, https://www.ljll.math.upmc.fr/perthame/coursM2.pdf.
- [21] B. Perthame, F. Quiròs, and J.-L. Vàzquez, The Hele-Shaw asymptotics for mechanical models of tumor growth, Arch. Ration. Mech. Anal., 212 (2014), pp. 99–127.
- [22] B. PERTHAME, M. TANG, AND N. VAUCHELET, Traveling wave solution of the Hele-Shaw model of tumor growth with nutrient, Math. Models Methods Appl. Sci., 24 (2014), pp. 2601–2626.
- [23] B. PERTHAME AND N. VAUCHELET, Incompressible limit of mechanical model of tumor growth with viscosity, Philos. Trans. A, 373 (2015), 20140283.
- [24] M. TANG, N. VAUCHELET, I. CHEDDADI, I. VIGNON-CLEMENTEL, D. DRASDO, AND B. PERTHAME, Composite waves for a cell population system modeling tumor growth and invasion, Chin. Ann. Math. Ser. B, 34 (2013), pp. 295–318.
- [25] M. RADSZUWEIT, M. BLOCK, J. G. HENGSTLER, E. SCHÖLL, AND D. DRASDO, Comparing the growth kinetics of cell populations in two and three dimensions, Phys. Rev. E, 79 (2009), 051907.
- [26] T. ROOSE, S. CHAPMAN, AND P. MAINI, Mathematical models of avascular tumour growth: A review, SIAM Rev., 49 (2007), pp. 179–208.
- [27] J. RANFT, M. BASANA, J. ELGETI, J.-F. JOANNY, J. PROST, AND F. JÜLICHER, Fluidization of tissues by cell division and apoptosis, Proc. Natl. Acad. Sci. USA, 107 (2010), pp. 20863– 20868.
- [28] J. L. VAZQUEZ, The Porous Medium Equation: Mathematical Theory, Oxford Scholarship Online, 2007, doi:10.1093/acprof:oso/9780198569039.001.0001